Giant pressure dependence and dimensional crossover in a metal-organic Heisenberg antiferromagnet

Björn Wehinger,[1,2,*] Christoph Fiolka,[3] David Graf,[4] William A. Coniglio,[4] Audrey Grockowiak,[4] Jyong-Hao Chen,[5,6] Jan Gukelberger,[6,7] Markos Skoulatos,[8] Karl Krämer,[3] Stan Tozer,[4] Christopher Mudry,[5] and Christian Rüegg[1,2]

[1] *Department of Quantum Matter Physics, University of Geneva, 24, Quai Ernest Ansermet, CH-1211 Genève, Switzerland*

[2] *Laboratory for Neutron Scattering and Imaging, Paul Scherrer Institute, CH-5232 Villigen PSI, Switzerland*

[3] *Department of Chemistry and Biochemistry, University of Bern, Freiestrasse 3, CH-3012 Bern, Switzerland*

[4] *National High Magnetic Field Laboratory, 1800 E. Paul Dirac Drive, Tallahassee, FL 32310, USA*

[5] *Condensed Matter Theory Group, Paul Scherrer Institute, CH-5232 Villigen PSI, Switzerland*

[6] *Theoretical Physics, ETH Zürich, CH-8093 Zürich, Switzerland*

[7] *Département de Physique and Regroupement québécois sur les matériaux de pointe, Université de Sherbrooke, Sherbrooke, Québec, J1K 2R1, Canada*

[8] *Heinz Maier-Leibnitz Zentrum and Physics Department, Technische Universität München, Lichtenbergstr. 1, D-85748 Garching, Germany*

(Dated: June 28, 2016)

Abstract

Square-lattice Heisenberg antiferromagnets with magnetic exchange couplings of the order of a few Kelvin can be realized in metal-organic materials. Here, we report on high-precision susceptibility measurements of the quasi-two-dimensional square-lattice Heisenberg antiferromagnet $(CuF_2(H_2O)_2)_2$-pyrazine in high magnetic fields and at high pressures using a tunnel diode oscillator. A continuous change of the magnetic exchange couplings by a factor of 3.3 is observed upon application of external pressure. This change causes a dimensional crossover of the magnetic properties from quasi-two dimensions via three dimensions to quasi-one dimension. The pressure-dependence of the characteristic microscopic magnetic energy scales and magnetic response are computed by combining first principle calculations using spin-polarized density functional theory and Quantum Monte Carlo simulations. The giant pressure effect together with the computational benchmarks enable the design and control of magnetic properties in a diverse class of metalorganic materials over a large range of energy scales and dimensionalities.

Designed quantum materials offer a fertile playground for the study of fundamental concepts in condensed matter physics and for potential applications in quantum technologies. Quantum effects are particularly strong in one and two dimensions, where intriguing new phenomena can arise from quantum many-body physics[1,2]. Materials with such structures can be created by chemical synthesis or nanotechnology.

Metal-organic materials based on coordination polymers with a metal-pyrazine network exhibit magnetic exchange couplings of only a few Kelvin that are strongly anisotropic in space[3,4]. Such insulating magnets are model systems for low-dimensional quantum magnetism because the magnetic exchange couplings can be determined with high accuracy and measurements of spin excitations are possible with currently available experimental techniques. Furthermore, the magnetic exchange couplings can be significantly modified by chemical variation of ligands and counter ions, fine-tuned by isotopic substitution, and the dimensionality of magnetic exchange can be chosen by preferential inhibition[5–8]. Applying external pressure provides a further direct tool to control structural and, in turn, magnetic properties[9–11].

In this study, we compress a single crystal of deuterated $(CuF_2(H_2O)_2)_2pyz$ – a model quasi-two dimensionsional (Q2D) square-lattice antiferromagnet – and report on magnetic susceptibility measurements using a Tunnel Diode Oscillator (TDO). The measured susceptibilities are then confronted with results from Quantum Monte Carlo (QMC) simulations and the pressure evolution of the electronic structure and magnetic couplings were investigated by density functional theory (DFT). We show that the application of external pressure continuously tunes the Heisenberg exchange couplings in $(CuF_2(H_2O)_2)_2pyz$ by more than a factor of three, thereby allowing for direct control of the dimensionality and enabling a continuous dimensional crossover. The observed continuous change is very large in comparison to what is reported for organic and inorganic materials under application of comparable external pressures[10,12].

As with other coordination polymers of the $(CuF_2(H_2O)_2)_nX$ family, the localized spins are carried by Cu^{2+} ions. They have a distorted octahedral coordination with equatorial F- and H_2O ligands. OH$\cdots$F hydrogen bonds link the Cu^{2+} complexes to layers parallel to the b-c plane, see Figure 1. The main magnetic exchange energy J arises from Cu-O-H$\cdots$F-Cu super-exchange paths which build Q2D magnetic layers[13]. In $(CuF_2(H_2O)_2)_2pyz$ two of these $CuF_2(H_2O)_2$ layers are linked by axial water ligands towards a double layer. Pyz ligands

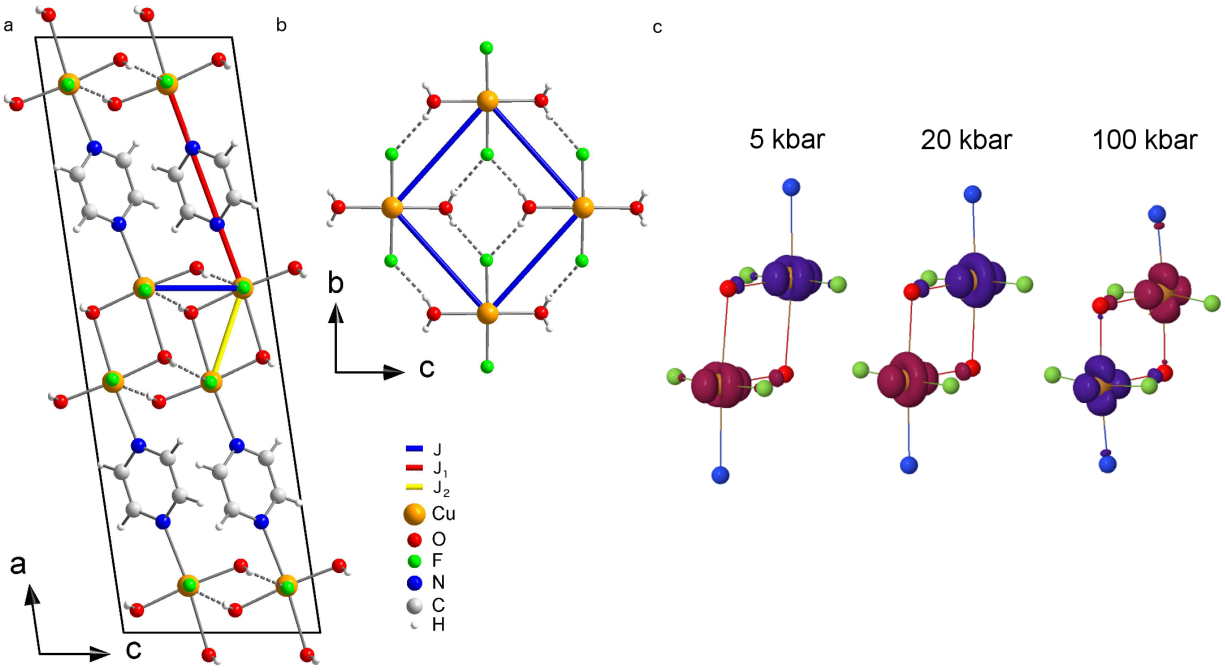

FIG. 1. View onto the crystallographic structure of $(CuF_2(H_2O)_2)_2pyz$ (a) along the b-axis and (b) onto the b-c plane. Cu^{2+} complexes with equatorial F- and H_2O ligands are linked by OH···F hydrogen bond parallel to the b-c plane. The H_2O ligands further connect two layers into a double layer by axial coordination. Pyz molecules occupy the second axial position and link the double layers into a 3D coordination network. The magnetic interaction J within the layer is mediated by superexchange via Cu-O-H···F-Cu paths, cf. (b). The weaker interactions J_2 within the double layer proceeds via Cu(equatorial-O-Cu(axial) bonds and J_1 between the double layers over the long Cu(axial)-pyz-Cu(axial) path. Copper atoms are magnified in (a) and (b) for better visualization. (c) The calculated spin-density distribution of the ground state is shown for various pressures, positive in red and negative in blue.

occupy the other axial position and connect along the a-axis to a 3D coordination network. The weaker magnetic exchange couplings J_1 and J_2 are located along these Cu(axial)-pyz-Cu(axial) and Cu(equatorial)-O-Cu(axial) pathways, respectively[11].

RESULTS

Single crystal magnetic susceptibility measurements in fields up to 35 T were performed at the National High Magnetic Field Laboratory (Tallahassee, Florida, USA) using a Tun-

nel Diode Oscillator (TDO) as a susceptometer, as described in the Methods. In order to probe the influence of external pressure, we compress isotropically a deuterated $(CuF_2(H_2O)_2)_2$pyz single crystal aligned with the crystallographic axis a parallel to the magnetic field. We have performed two independent experiments, where we used (i) a piston cylinder cell for pressures up to 17.9 kbar in fields up to 35 T and a minimum temperature of 1.5 K and (ii) a specially designed Moissanite anvil cell for pressures up to 37.1 kbar in fields up to 18 T and a minimum temperature of 0.4 K.

The pressure-dependence of the TDO resonance frequency as function of magnetic field and a constant temperature of 1.5 K are shown in Figure 2a. The magnetic susceptibility $\chi = \frac{\partial M}{\partial H}$ is obtained by subtracting the magnetoresistive background of the resonator coil from the resonance frequency and is presented in Figure 2b. A spin-flop transition is observed at low fields, see insert of Figure 2b. The transition appears at 1.2 T at a pressure of 1.5 kbar and shifts to slightly lower fields for increased pressure (1.0 T at 17.9 kbar). The susceptibility increases with growing external field and shows a pronounced peak prior to saturation. The shape of the susceptibility including the spin-flop transition is compared to QMC simulations and discussed further below. The magnetization is derived from the susceptibility by numerical integration and shown in Figure 2c. For fields below the spin-flop transition, the magnetization increases very little with increasing field. Beyond the first transition the spins gradually align with increasing magnetic field up to saturation. The saturation field B_c changes significantly upon pressure whereas the shape of magnetization remains similar, see Figure 2c and 3a. The Néel temperatures T_N were determined for each pressure point by a temperature dependent measurement of the resonance frequency at the spin-flop field and are reported in Figure 3b. The choice of applying this particular external field allows a precise measurement of the Néel temperature because the change of the resonance frequency as a function of temperature is well pronounced. The change upon pressure is also drastic. The saturation field is proportional to the arithmetic average of the exchange couplings per spin,

$$J + \frac{1}{2}J_\perp = B_c g \mu_B / 4, \tag{1}$$

were μ_B is the Bohr magneton, $g = 2.42$ the experimentally determined g-factor along the applied field[11] and $J_\perp$ the arithmetic sum of J_1 and J_2. A linear fit to the experimental values results in $J + \frac{1}{2}J_\perp = 11.48\,\text{K} - 0.34\,\text{K/kbar}\cdot p$ for pressures up to 18 kbar and $J + \frac{1}{2}J_\perp = 7.14\,\text{K} - 0.09\,\text{K/kbar}\cdot p$ for higher pressures. Such a strong pressure dependence is highly

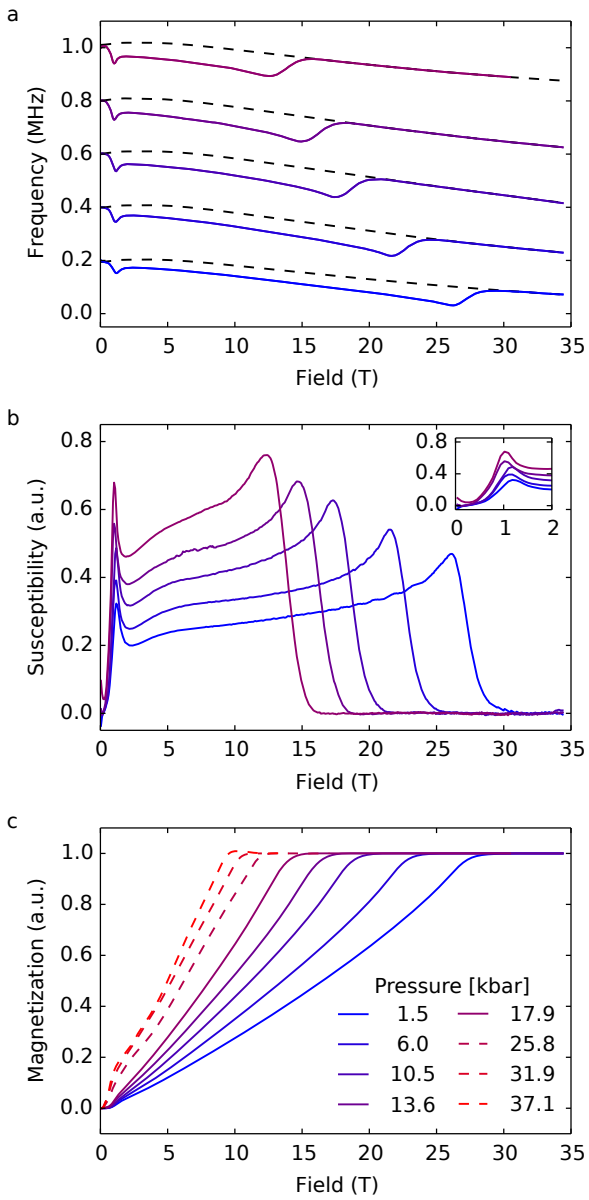

FIG. 2. (a) Measured resonance frequencies of the tunnel diode oscillator (TDO) at selected pressures and a temperature of 1.5 K (full lines) together with the corresponding magnetoresistive background of the resonator coil (dashed lines). The pressures are 17.9, 13.6, 10.5, 6.0 and 1.5 kbar from top to bottom. (b) Magnetic susceptibility for the same pressures and temperature. The insert shows a magnification of the spin-flop transition. (c) Magnetization at 37.1, 31.9 and 25.8 kbar (dashed lines from left to right) and for the pressures shown in panel (a) and (b) (full lines).

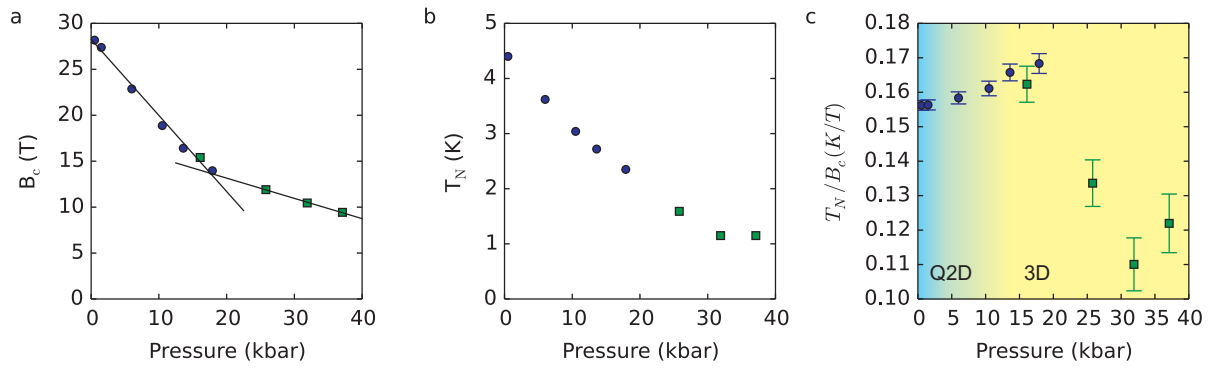

FIG. 3. Measured saturation field B_c (a) and Néel temperatures T_N (b) as function of external pressure. The blue circles were obtained form measurements using the piston cell and the green squares result from the experiment employing the Moissanite cell. Linear fits to B_c are shown as black lines. (c) Ratio T_N/B_c versus external pressure. The dimensional crossover is illustrated by colors: the system continuously transforms from Q2D (blue) to 3D (yellow) with closest isotropic realization at the maximum around p=18 kbar.

unusual and much stronger than what is usually observed in materials.

For the lowest pressures we assume the Heisenberg interlayer exchange couplings J_1 and J_2 to be much smaller than the in-plane exchange coupling. This assumption is justified by inelastic neutron scattering performed at SINQ, Paul Scherrer Institute, Switzerland and the first principle calculations discussed further below. This allows the simple relation $J \approx B_c g\mu_B/n$ ($n = 4$ is the number of nearest neighbors) and results in $J = 11.45$ K at 0.5 kbar and 11.13 K at 1.5 kbar. We note that the deuterated single crystal samples used for both neutron scattering and magnetic susceptibility measurements may have marginally different exchange couplings compared to protonated samples. However, such an isotope effect is small[6] and not investigated within this study. Given J and T_N, we can estimate the Heisenberg interlayer exchange coupling. Random Phase Approximation (RPA) was employed to relate the in-plane Heisenberg exchange coupling and the Néel temperature to the interlayer coupling. By assuming a uniform Heisenberg exchange coupling along the stacking direction we evaluate the dynamic susceptibility by a mean-field treatment[14], see the Methods. For an isotropic square-lattice Heisenberg antiferromagnet with weak inter-plane

coupling, we find

$$|J_\perp| = \frac{J^2}{2c_2 T_N} e^{-4\pi\rho_s/T_N} \tag{2}$$

where c_2 is a non-universal constant and ρ_s is the spin stiffness. We use the numerical value $c_2 = 0.044$ estimated by QMC simulations for a spin 1/2 system[15] and $\rho_s = J/4$. At a pressure of 1.5 kbar we obtain $|J_\perp| = 0.095 \pm 0.015$ K.

Experimental evidence for the dimensional crossover is illustrated in Figure 3c, where we plot the ratio T_N/B_c versus pressure. Simple mean-field arguments would predict both T_N and B_c to be proportional to the sum of coupling constants and hence their ratio to be constant. With reduced dimensionality, however, fluctuations become more important and suppress T_N in the 2D and 1D limits.

For intermediate situations with finite T_N the ratio T_N/B_c takes also finite values with a maximum for the 3D isotropic case ($J_\perp/J = 1$). At zero pressure our system is Q2D and the observed increase of T_N/B_c with pressure until 18 kbar thus implies an increase of $J_\perp/J$. Assuming a further increase of $J_\perp/J$ beyond the maximum in T_N/B_c together with the observed decrease of T_N/B_c requires that the system becomes more anisotropic towards a Q1D system. The pressure dependence of the Heisenberg exchange couplings is further investigated by *ab inito* calculations, as discussed below. They confirm the assumption that $J_\perp/J$ increases further for pressures beyond the one at which the maximum of T_N/B_c is observed.

QMC simulations were performed using stochastic series expansion with generalized directed loop updates, as provided by the ALPS open-source codes[16–21]. A nearest-neigbour anisotropic XXZ Hamiltonian with spin-1/2 localized on the sites of a simple cubic lattice was assumed. Nearest-neigbour pairs of spin-1/2 within any layer perpendicular to the stacking direction are coupled antiferromagnetically with isotropic Heisenberg exchange coupling J. Consecutive layers are coupled alternatively with ferromagnetic and antiferromagnetic Heisenberg exchange couplings of magnitude $|J_\perp|$. The spin $SU(2)$ symmetry was broken to $U(1)$ by an easy axis anisotropy in the inter-layer couplings $|J_\perp^z| > |J_\perp|$, see the Methods. Calculated susceptibility and magnetization are compared to experiment at a pressure of 1.5 kbar in Figure 4. The QMC simulations help understanding the shape of the susceptibility. The spin-flop transition could be reproduced using the value $|J_\perp^z| = 0.19$ K. Both susceptibility and magnetization are in excellent agreement with the experimental data.

The microscopic mechanism behind the giant pressure dependence is investigated by

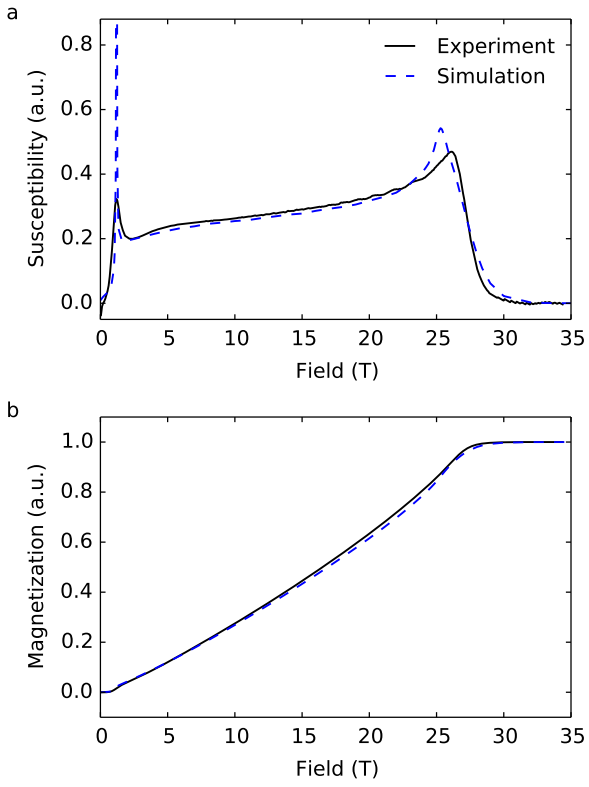

FIG. 4. Magnetic susceptibility (a) and magnetization (b) at a pressure of 1.5 kbar and a temperature of 1.5 K as obtained from experiment (full line) and QMC simulations (dashed line). The stochastic error (one standard deviation) on the QMC susceptibility is 5 % at the spin-flop transition and < 0.3 % elsewhere.

electronic structure calculations from first principle. We used spin polarized DFT as implemented in the CASTEP code[22,23]. The generalized gradient approximation was employed using the exchange correlation functional of Perdew, Burke and Ernzerhof (PBE) within the plane-wave formalism and norm-conserving pseudo-potentials of the optimized form[24,25], see the Methods for further details. Heisenberg exchange couplings were estimated by total energy calculations for different spin configurations. The calculated spin density distribution for the optimized geometries at different pressures and the magnetic exchange paths are depicted in Fig. 1. The calculation confirms that the in-plane Heisenberg exchange coupling is governed by the hydrogen bonded Cu-O-H$\cdots$F-Cu super-exchange path, estimated to 43.8 K at 1.5 kbar. The Q2D layers are coupled through nearest-neigbour Heisenberg exchange couplings that are alternatively antiferromagnetic and ferromagnetic. The inter-layer

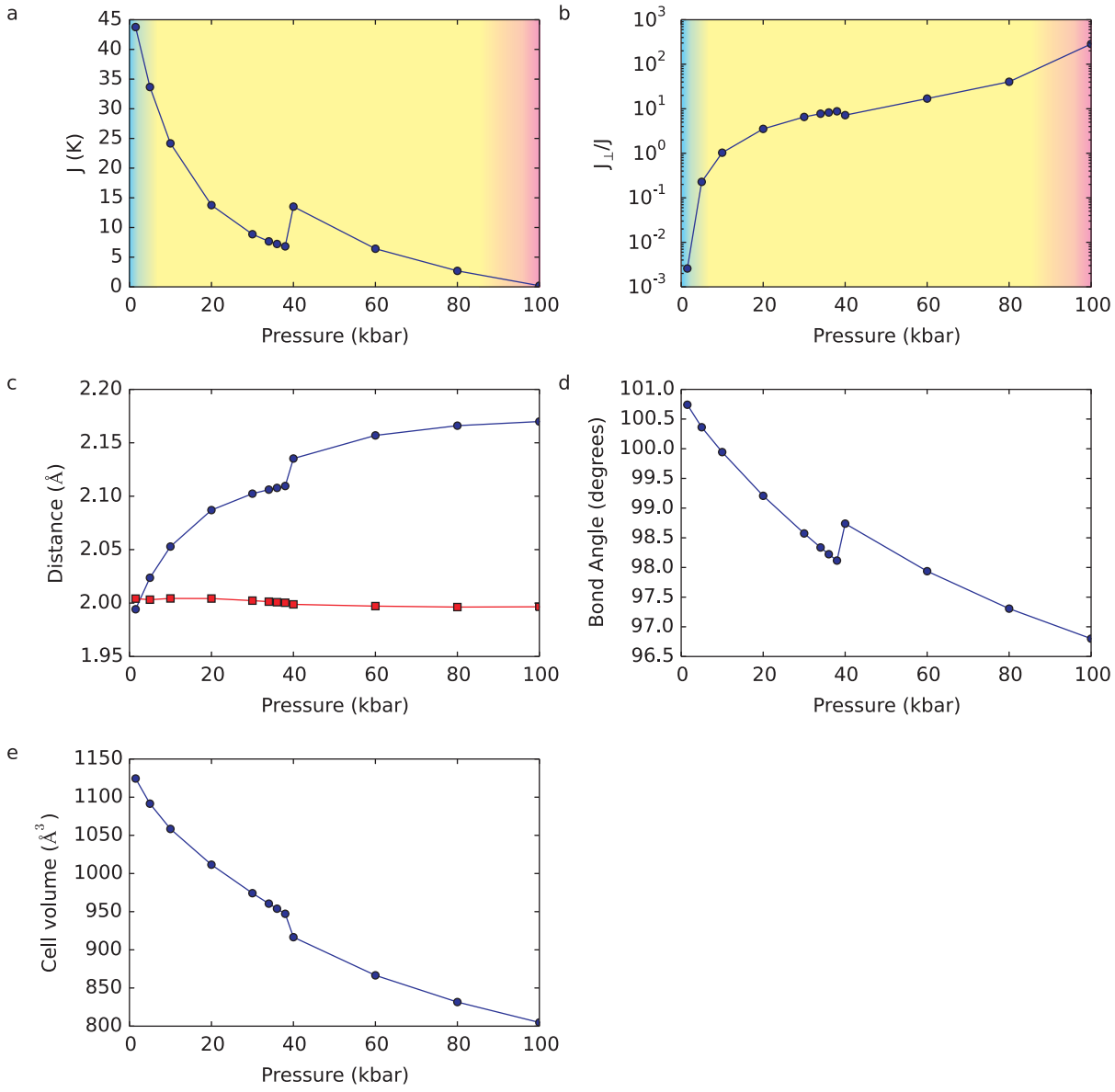

FIG. 5. *Ab initio* calculated magnetic and structural parameters of $(CuF_2(H_2O)_2)_2pyz$ as function of isotropic external pressure: (a) J, (b) $J_\perp/J$, (c) bond lengths of Cu-F (connected blue dots) and Cu-O (connected red squares), (d) bond angle of the water bridged Cu-O-Cu path, and (e) cell volume.

Heisenberg exchange coupling within a double layer, connected as it is via the water bridges, is governed by the Cu-O-Cu path. This coupling is found to be ferromagnetic in the calculations performed at a pressure of 1.5 kbar and below and turns out to be antiferromagnetic at all higher pressures. The Heisenberg exchange coupling between two consecutive double

layers is realized via the pyrazine building block connecting two Cu atoms, see Figure 1a. It is antiferromagnetic up to a pressure of 1.5 kbar, becomes ferromagnetic for higher pressures up to 80 kbar, and is again antiferromagnetic for pressures beyond 100 kbar. Applying isotropic external pressure leads to a continuous deformation of the spin density distribution, see Figure 1c. The spin density along the Cu-F bond is redistributed orthogonal to it along the Cu-N bonds. The shape of the spin density around the Cu atoms resembles a squeezed torus at 5 kbar, while it forms a more uniform torus at 20 kbar. At 100 kbar there is very little spin density left along the Cu-F bonds and both inter-layer Heisenberg exchange couplings become antiferromagnetic.

The estimated pressure dependence of J and the ratio $J_\perp/J$ are presented in Figure 5a and b. The pressure dependence of J is in good agreement with the experiment: J decreases upon application of isotropic external pressure by more than a factor of three within the measured pressure range and continues to decrease all the way up to 100 kbar. Both the ferromagnetic and antiferromagnetic inter-layer Heisenberg exchange couplings increase significantly with pressure. At around 10 kbar $J_\perp$ increases to a strength comparable to J. The systematic error of $J_\perp$ is different from the error of J, absolute values of the plotted ratio $J_\perp/J$ are thus not reliable. However, the first principle calculations identify a clear trend. $J_\perp/J$ increases rapidly for low pressures and the system becomes 3D and finally Q1D.

The deformation of the spin density is accompanied by an increase of the Cu-F bond length with pressure while the Cu-O bond length undergoes very little change, see Figure 5c. The angle of the water bridged exchange becomes smaller, as the layers are pushed together with pressure, see Figure 5d. We identify discontinuities in the pressure dependence of structural parameters indicating electronic phase transitions, see Figure 5c-e. The observed transitions lead to discontinuities in the exchange parameters, of which one at 40 kbar is well pronounced. It corresponds to a first-order phase transition of the orbital orientation. At this pressure J is of the same order of magnitude as the calculated values for J_1 (water bridged) and J_2 (pyz connection) and the model is 3D below and above the transition. At 100 kbar both interlayer couplings exceed J. The resulting magnetic properties are those of weakly antiferromagnetic coupled quantum spin-1/2 chains. The transitions of the interlayer couplings from ferromagnetic-antiferromagnetic to antiferromagnetic-ferromagnetic at around 1.5 kbar and finally to antiferromagnetic-antiferromagnetic at 100 kbar are also discontinuous, but this is not resolved by the current calculation.

DISCUSSION

The results unequivocally point to a continuous evolution of the dimensionality of magnetic properties in $(CuF_2(H_2O)_2)_2$pyz under application of isotropic external pressure. The direct evidence for the dimensional crossover can be seen from the pressure dependence of T_N/B_c, see Figure 3c. The assumption made to transcend these data – the further increase of $J_\perp/J$ beyond the maximum – is confirmed by the *ab initio* calculation, see Figure 5b. The magnitude of the nearest-neighbor inter-layer Heisenberg exchange coupling $|J_\perp|$ was extracted from the experimental data with help of a formula derived from a mean field treatment assuming $J \gg J_\perp$. The obtained ratio $J_\perp/J$ compares reasonably well with the estimation from the *ab initio* calculation at ambient pressure. There is no symmetry argument which requires the magnitudes of the two exchange couplings along the stacking direction J_1 and J_2 to be identical. However, the DFT calculations indicate values of the same order of magnitude. Assuming $J_1 = -J_2$ allows us to extract an average value from the available experimental data and to reduce the number of free parameters. For increasing pressures, the DFT calculations show a rapid increase of $J_\perp/J$ and the approximations used in the RPA are less justified when the system becomes more 3D. In fact, Equation 2 would require an increase of T_N for increasing $J_\perp/J$, contradicting the experimental observation. We thus conclude that the assumption $J \gg J_\perp$ used in the mean field treatment is valid for ambient pressure only. The susceptibility can be well reproduced by QMC simulations. This confirms that the system can be described by a Heisenberg antiferromagnet with XXZ symmetry in spin space and anisotropic Heisenberg exchange couplings along the nearest-neighbor bonds of a cubic lattice. The shape of the susceptibility and magnetization is rather insensitive to changes from Q2D to 3D but would differ significantly when changed to Q1D[7].

The electronic structure calculations explain the drastic evolution of the exchange parameters upon application of isotropic external pressure by a continuous deformation of the spin density distribution around the Cu atoms accompanied by an anomalous increase of the Cu-F bond length. At even higher pressures the magnetic exchange coupling is dominated by the Cu-O-Cu and Cu-pyz-Cu exchange path. The system is thus expected to become Q1D by realizing weakly coupled antiferromagnetic spin chains. Susceptibility measurements at pressures up to 100 kbar and more are accesible to future experiments using non-magnetic

diamond anvil cells.

The magnitudes of the Heisenberg exchange couplings are significantly overestimated by our *ab initio* calculations but the relative pressure dependence is correctly described. The overestimation can be attributed in large part to the limitations in the employed exchange-correlation-term within PBE. In fact, the Copper d orbitals are rather well localized which leads to strong on-site correlations. An appropriate correction could be envisaged by extending the *ab initio* calculation by a Hubbard U model (DFT+U) or by including dynamical mean-field correlations (DFT+DMFT methods). Due to these limitations in the exchange-correlation functional there is also a systematic uncertainty in the calculated pressure. An experimental investigation of the structural parameters, such as cell volume and atomic position, as function of pressure would thus provide very important information to calibrate the calculated results, see Figure 5.

$(CuF_2(H_2O)_2)_2$pyz will be a very important model system to benchmark the limitations of new theoretical approaches describing the spin dynamics across dimensional crossovers. Magnetic excitations can be measured, for example, using neutron spectroscopy where experiments can be conducted at relevant pressure-temperature conditions and applied magnetic field. Neutron scattering experiments under pressure will allow for accurate determination of the full set of exchange parameters with high accuracy. $(CuF_2(H_2O)_2)_2$pyz comprises an excellent model system to study correlated electron physics and superconductivity when doped with holes or electrons. The chemical flexibility is particularly high in this metal-organic compounds and it will thus be possible and very promising to realize a charge doped quantum magnet with extraordinary pressure dependence. From a material science perspective such materials are very interesting. In fact, they not only provide the possibility to engineer tuneable quantum materials with desired properties exploiting state-of-the-art chemistry, but also provide indispensable benchmarks for testing the most recent advances in the quantum many-body physics of low-dimensional systems and calculating magnetic properties from first principle.

In summary, we have shown that the Heisenberg exchange couplings in the model square-lattice antiferromagnet $(CuF_2(H_2O)_2)_2$pyz can efficiently be tuned by external pressure. The system is well described by a spin-1/2 Heisenberg XXZ Hamiltonian with exchange couplings in the range of a few Kelvin in magnitude. The effective dimensionality with regard to magnetic properties can be changed continuously through the great sensitivity of the Heisenberg

exchange couplings to pressure. At ambient pressure the Heisenberg exchange couplings are dominated by the antiferromagnetic hydrogen bonded Cu-O-H$\cdots$F-Cu super-exchange path in two dimensions. The Q2D layers are weekly coupled along the third (stacking) dimension with alternating ferro- and antiferromagnetic Heisenberg exchange couplings. Upon application of external pressure, the spin density is continuously deformed. This effect is accompanied by an increase of the Cu-F distance. The inter-layer Heisenberg exchange coupling increases relative to the intra-layer one. Magnetic properties become increasingly 3D. At more elevated pressures the Heisenberg exchange couplings are predicted to continuously transform so as to effectively realize weakly coupled antiferromagnetic spin-1/2 chains. The accurate control of the crossover regime between different dimensionalities offers new opportunities in materials design and allows for the study of exotic quantum phenomena realized in such situations. The employed approach combining modern materials chemistry with recently developed quantum many body simulation tools provides a promising strategy for designing quantum materials with remarkable properties.

METHODS

Sample

Deuterated $(CuF_2(H_2O)_2)_2pyz$ single crystals were grown similar to the method described in Reference[11]: Two equivalents of ammonium fluoride (7.122 g, 92 mmol) and one equivalent of pyrazine (7.689 g, 96 mmol) were dissolved in 96 ml water. A filtered solution of copper(II) nitrate made from one equivalent copper(II) chloride (12.907 g, 96 mmol) and two equivalents silver(I) chloride (32.616 g, 192 mmol) in 96 ml water was added at 5° C. Upon slow evaporation at first place $CuF_2(H_2O)_2pyz$ crystals form and after several months $(CuF_2(H_2O)_2)_2pyz$ grew epitactic on the first compound. Single crystals of $(CuF_2(H_2O)_2)_2pyz$ were separated and checked by powder x-ray diffraction for phase purity. The samples were stored in the mother liquor.

Tunnel diode oscillator measurements

The TDO susceptometer consists of an oscillator circuit with a tunnel diode and a resonant LC circuit with the sample inside the inductor. Neglecting small parasitic components

and lengths, oscillation frequency is proportional to $\omega = 1/\sqrt{LC}$, where L is modified by the susceptibility of the sample inside it[26–28]. Measurements using the piston cell were performed at the National High Magnetic Field Laboratorys 35 T, 32 mm bore resistive magnet in cell 12. The inductor was a single layer coil, 800 μm in diameter, 25 turns, wound with 28 μm wire. The piston cell was cooled by a He^4 cryostat with variable temperature insert where the flow of He gas entering the sample area from a valve at the base of the instrument controls the temperature. The measurements were performed at a temperature of 1.5 K and pressures 0.5, 1.5, 6.0, 13.6, and 17.9 kbar. The experiments at higher pressures were performed using a Moissanite anvil cell with 800 μm culets, see[29] for similar design. Here, the resonator coil was 150 μm in outer diameter, 3 turns, with 14 μm diameter copper wire (with insulation). The measurements were performed in the NHMFL superconducting magnet system SCM 2 in a He^3 system where the base temperature is reached by condensing He^3 gas to liquid by using a 1 K pot. These measurements were performed at a temperature of 0.4 K and pressures 16.1, 25.8, 31.9 and 37.1 kbar. Daphne 7474 was used as pressure transmitting medium and the pressure was determined *in situ* from the fluorescence of a ruby crystal.

Monte Carlo simulations

For the QMC simulations, the material is modeled as a spin-1/2 system on a simple cubic lattice with a two-site unit cell

$$\widehat{H}_{\text{spin}} := \sum_{\boldsymbol{n}} \sum_{a=x,y,z} \left(J \sum_{m} \sum_{\mu=1}^{2} \widehat{S}^a_{\boldsymbol{n},m} \widehat{S}^a_{\boldsymbol{n}+\boldsymbol{\delta}_\mu,m} + \sum_{m\,\text{odd}} J_1^a \widehat{S}^a_{\boldsymbol{n},m} \widehat{S}^a_{\boldsymbol{n},m+1} + \sum_{m\,\text{even}} J_2^a \widehat{S}^a_{\boldsymbol{n},m} \widehat{S}^a_{\boldsymbol{n},m+1} - \sum_{m} h^a_{\boldsymbol{n},m} \widehat{S}^a_{\boldsymbol{n},m} \right). \tag{3}$$

Here $\boldsymbol{n}$ is a two-dimensional vector associated to a site in a layer, while m is the index along the stacking direction of the layers. The label $a\,(= x, y, z)$ enumerates the spin components. We choose the z-direction to correspond to the crystallographic a-axis, which is aligned with the magnetic field, i.e. $h^z_{\boldsymbol{n},m} = h$ and $h^x_{\boldsymbol{n},m} = h^y_{\boldsymbol{n},m} = 0$. The intra-layer coupling constant J=11.13 K, inter-layer coupling $J_1^{x,y} = -J_2^{x,y} = J_\perp = 0.09$ K and the g-factor g=2.42 have been set to the values deduced from the saturation field, the Néel temperature, and the reported value for g[11], respectively, at 1.5 kbar. Finally, the easy-axis anisotropy

$J_1^z = -J_2^z = J_\perp^z$ has been chosen such that the observed spin-flop field $B_{sf} \approx 1.2\,\mathrm{T}$ is reproduced. For each field value shown in Fig. 4, 10 000 Monte Carlo sweeps were performed for thermalization and 800 000 sweeps after thermalization. The spin-flop transition is sensitive to finite size effects and a rather large number of spins are required for a correct description. We thus computed the susceptibility, magnetization, binder cumulant, energy and their auto-correlation times for various system sizes at the transition and verified that the value of the transition field B_{sf} is converged with system size to within 0.05 T for the chosen system containing $32 \times 32 \times 32$ spins.

Ab initio calculations

The pseudopotentials used in this study were generated using the Vanderbilt scheme with single projectors. Valence configuration, core radii and cut-off wave vectors for the different species were taken from the pseudopotential data base of the Rappe Group[25,30]. A plane wave cut-off of 1500 eV and an electronic grid sampling on a $2 \times 2 \times 3$ Monkhorst-Pack grid ensured convergence of forces to < 1.0 meV/Å. The total energy was converged to 0.1 meV for each spin configuration. The cell geometry was optimized employing the Broyden-Fletcher-Goldfarb-Shannon method by varying lattice and internal parameters[31].

Random Phase Approximation for Quasi-Two-Dimentional Susceptibilities

Following the section of Monte Carlo simulations, we consider the Hamiltonian Eq. 3

$$\widehat{H}^{(3d)}_{\text{source}} := \widehat{H}_{\text{spin}}, \tag{4}$$

where the exchange coupling J_1^a and J_2^a can be either positive or negative. The real-valued numbers $h^a_{\boldsymbol{n},m}$ are sources that allow to compute any spin-spin correlation function. If chosen independent of $\boldsymbol{n}$ and m, they are proportional to an applied external uniform magnetic field.

We may ignore the quantum character of the spin operators implied by the symbol hat in $\widehat{S}^a_{\boldsymbol{n},m}$ in the mean-field (classical) approximation. For simplicity, we assume that the exchange couplings are isotropic, namely $J_1^a \equiv J_1$ and $J_2^a \equiv J$ are independent of the index a. If

$$|J| \;\gg\; |J_1|\,,\, |J_2| \;\geq 0\,, \tag{5}$$

we may then perform a mean-field approximation by which the full three-dimensional problem is truncated down to an effective (eff) two-dimensional problem

$$H^{(3d)}_{\text{source}} \;\rightarrow\; \sum_{m\,\text{odd}} H^{(2d)}_{\text{eff-source},m\,\text{odd}} \;+\; \sum_{m\,\text{even}} H^{(2d)}_{\text{eff-source},m\,\text{even}}\,. \tag{6}$$

By choosing the external source to be of the plane-wave type and by employing linear-response theory, the three-dimensional susceptibility $\chi^{3d}_{\boldsymbol{q}_\parallel,q_\perp}$ is approximated by

$$\chi^{3d}_{\boldsymbol{q}_\parallel,q_\perp} \approx \chi^{3d,\text{RPA}}_{\boldsymbol{q}_\parallel,q_\perp} := \frac{\chi^{2d}_{\boldsymbol{q}_\parallel}\left[1-(J_1+J_2)\,\cos q_\perp\,\chi^{2d}_{\boldsymbol{q}_\parallel}\right]}{1-\left(J_1^2+J_2^2+2J_1J_2\,\cos 2q_\perp\right)\left(\chi^{2d}_{\boldsymbol{q}_\parallel}\right)^2}\,, \tag{7}$$

where $\boldsymbol{q} \equiv (\boldsymbol{q}_\parallel, q_\perp)$ is the wave vector, $\perp$ indicates the direction perpendicular to the two-dimensional layer, namely along the stacking direction. With the explicit form of the two-dimensional antiferromagnetic susceptibility $\chi^{2d}(T)$ as a function of temperature T[15,32]

$$\chi^{2d}(T) \approx c_2 \frac{T}{J^2}\, e^{4\pi\rho_s/T}\,, \tag{8}$$

we can solve the pole equation for $J_1 = -J_2 = J_\perp$ and obtain

$$T_N = \frac{4\pi\rho_s}{-\ln 2c_2 - \ln\frac{|J_\perp|}{J} - \ln\frac{T_N}{J}}\,, \tag{9}$$

which can be reformulated to Eq. 2. Solving the pole equation for $J_1 = J_2 = J_\perp$ also leads to Eq. 9 and agrees with previously published results[15].

ACKNOWLEDGMENT

We thank Robert Schwartz for professional engineering of the pressure cells and fixtures used for this study and acknowledge Thierry Giamarchi for fruitful discussions. The computations were performed at University of Geneva on the Baobab cluster and resources of the Theory of Quantum Matter Group. We have received funding from the European Community's Seventh Framework Programme (FP7/2007-2013) under grant agreement no. 290605 (PSI-FELLOW/COFUND) and the Swiss National Science Foundation (SNSF) under grant no. 200020_150257 and SINERGIA Network Mott Physics Beyond the Heisenberg Model. J.G. was supported by an SNSF Early Postdoc.Mobility fellowship during part of this work and M.S. by TRR80 of the German physical society (DPG). We furthermore acknowledge funding for the high field measurements at the National High Magnetic Field Laboratory,

Tallahassee, Florida by grant No. DOE NNSA DE-NA0001979 and support by National Science Foundation Cooperative Agreement No. DMR-1157490 and the State of Florida.

---

* bjorn.wehinger@unige.ch

[1] E. Dagotto and T. M. Rice, Surprises on the way from one- to two-dimensional quantum magnets: The ladder materials, Science **271**, 618 (1996).

[2] B. Dalla Piazza, M. Mourigal, N. B. Christensen, G. J. Nilsen, P. Tregenna-Piggott, T. G. Perring, M. Enderle, D. F. McMorrow, D. A. Ivanov, and H. M. Ronnow, Fractional excitations in the square-lattice quantum antiferromagnet, Nat. Phys. **11**, 62 (2015).

[3] M. Conner, A. McConnell, J. Schlueter, and J. Manson, Structural and magnetic properties of copper(II) coordination polymers containing fluoride-based anions and ancillary organic ligands, Journal of Low Temperature Physics **142**, 273 (2006).

[4] P. A. Goddard, J. Singleton, P. Sengupta, R. D. McDonald, T. Lancaster, S. J. Blundell, F. L. Pratt, S. Cox, N. Harrison, J. L. Manson, H. I. Southerland, and J. A. Schlueter, Experimentally determining the exchange parameters of quasi-two-dimensional Heisenberg magnets, New Journal of Physics **10**, 083025 (2008).

[5] F. M. Woodward, P. J. Gibson, G. B. Jameson, C. P. Landee, M. M. Turnbull, and R. D. Willett, Two-dimensional heisenberg antiferromagnets: syntheses, x-ray structures, and magnetic behavior of $[Cu(pz)_2](ClO_4)_2$, $[Cu(pz)_2](BF_4)_2$, and $[Cu(pz)_2(NO_3)](PF_6)$, Inorganic Chemistry **46**, 4256 (2007), pMID: 17432847.

[6] P. A. Goddard, J. Singleton, C. Maitland, S. J. Blundell, T. Lancaster, P. J. Baker, R. D. McDonald, S. Cox, P. Sengupta, J. L. Manson, K. A. Funk, and J. A. Schlueter, Isotope effect in quasi-two-dimensional metal-organic antiferromagnets, Phys. Rev. B **78**, 052408 (2008).

[7] P. A. Goddard, J. L. Manson, J. Singleton, I. Franke, T. Lancaster, A. J. Steele, S. J. Blundell, C. Baines, F. L. Pratt, R. D. McDonald, O. E. Ayala-Valenzuela, J. F. Corbey, H. I. Southerland, P. Sengupta, and J. A. Schlueter, Dimensionality selection in a molecule-based magnet, Phys. Rev. Lett. **108**, 077208 (2012).

[8] T. Lancaster, P. A. Goddard, S. J. Blundell, F. R. Foronda, S. Ghannadzadeh, J. S. Möller, P. J. Baker, F. L. Pratt, C. Baines, L. Huang, J. Wosnitza, R. D. McDonald, K. A. Modic, J. Singleton, C. V. Topping, T. A. W. Beale, F. Xiao, J. A. Schlueter, A. M. Barton, R. D.

Cabrera, K. E. Carreiro, H. E. Tran, and J. L. Manson, Controlling magnetic order and quantum disorder in molecule-based magnets, Phys. Rev. Lett. **112**, 207201 (2014).

[9] J. L. Musfeldt, Z. Liu, S. Li, J. Kang, C. Lee, P. Jena, J. L. Manson, J. A. Schlueter, G. L. Carr, and M.-H. Whangbo, Pressure-induced local structure distortions in $Cu(pyz)F_2(H_2O)_2$, Inorganic Chemistry **50**, 6347 (2011), pMID: 21644536.

[10] S. Ghannadzadeh, J. S. Möller, P. A. Goddard, T. Lancaster, F. Xiao, S. J. Blundell, A. Maisuradze, R. Khasanov, J. L. Manson, S. W. Tozer, D. Graf, and J. A. Schlueter, Evolution of magnetic interactions in a pressure-induced Jahn-Teller driven magnetic dimensionality switch, Phys. Rev. B **87**, 241102 (2013).

[11] A. Lanza, C. Fiolka, M. Fisch, N. Casati, M. Skoulatos, C. Ruegg, K. W. Kramer, and P. Macchi, New magnetic frameworks of $[(CuF_2(H_2O)_2)x(pyz)]$, Chem. Commun. **50**, 14504 (2014).

[12] P. Merchant, B. Normand, K. W. Kramer, M. Boehm, D. F. McMorrow, and C. Ruegg, Quantum and classical criticality in a dimerized quantum antiferromagnet, Nature Physics **10**, 373 (2014).

[13] J. L. Manson, M. M. Conner, J. A. Schlueter, A. C. McConnell, H. I. Southerland, I. Malfant, T. Lancaster, S. J. Blundell, M. L. Brooks, F. L. Pratt, J. Singleton, R. D. McDonald, C. Lee, and M.-H. Whangbo, Experimental and theoretical characterization of the magnetic properties of $CuF_2(H_2O)2(pyz)$ (pyz = pyrazine): A two-dimensional quantum magnet arising from super-superexchange interactions through hydrogen bonded paths, Chemistry of Materials **20**, 7408 (2008).

[14] D. J. Scalapino, Y. Imry, and P. Pincus, Generalized Ginzburg-Landau theory of pseudo-one-dimensional systems, Phys. Rev. B **11**, 2042 (1975).

[15] C. Yasuda, S. Todo, K. Hukushima, F. Alet, M. Keller, M. Troyer, and H. Takayama, Néel temperature of quasi-low-dimensional heisenberg antiferromagnets, Phys. Rev. Lett. **94**, 217201 (2005).

[16] A. W. Sandvik and J. Kurkijärvi, Quantum monte carlo simulation method for spin systems, Phys. Rev. B **43**, 5950 (1991).

[17] A. W. Sandvik, Stochastic series expansion method with operator-loop update, Phys. Rev. B **59**, R14157 (1999).

[18] F. Alet, S. Wessel, and M. Troyer, Generalized directed loop method for quantum monte carlo simulations, Phys. Rev. E **71**, 036706 (2005).

[19] http://alps.comp-phys.org/.

[20] B. Bauer, L. D. Carr, H. G. Evertz, A. Feiguin, J. Freire, S. Fuchs, L. Gamper, J. Gukelberger, E. Gull, S. Guertler, A. Hehn, R. Igarashi, S. V. Isakov, D. Koop, P. N. Ma, P. Mates, H. Matsuo, O. Parcollet, G. Pawłowski, J. D. Picon, L. Pollet, E. Santos, V. W. Scarola, U. Schollwöck, C. Silva, B. Surer, S. Todo, S. Trebst, M. Troyer, M. L. Wall, P. Werner, and S. Wessel, The ALPS project release 2.0: open source software for strongly correlated systems, Journal of Statistical Mechanics: Theory and Experiment **2011**, P05001 (2011).

[21] A. Albuquerque, F. Alet, P. Corboz, P. Dayal, A. Feiguin, S. Fuchs, L. Gamper, E. Gull, S. Gürtler, A. Honecker, R. Igarashi, M. Körner, A. Kozhevnikov, A. Läuchli, S. Manmana, M. Matsumoto, I. McCulloch, F. Michel, R. Noack, G. Pawłowski, L. Pollet, T. Pruschke, U. Schollwöck, S. Todo, S. Trebst, M. Troyer, P. Werner, and S. Wessel, The ALPS project release 1.3: Open-source software for strongly correlated systems, Journal of Magnetism and Magnetic Materials **310**, 1187 (2007), proceedings of the 17th International Conference on Magnetism.

[22] S. Clark, M. Segall, C. Pickard, P. Hasnip, M. Probert, K. Refson, and M. Payne, First principles methods using CASTEP, Z. Kristallogr. **220**, 567 (2005).

[23] M. C. Payne, M. P. Teter, D. C. Allan, T. A. Arias, and J. D. Joannopoulos, Iterative minimization techniques for *ab initio* total-energy calculations: molecular dynamics and conjugate gradients, Rev. Mod. Phys. **64**, 1045 (1992).

[24] J. P. Perdew, K. Burke, and M. Ernzerhof, Generalized gradient approximation made simple, Phys. Rev. Lett. **77**, 3865 (1996).

[25] A. M. Rappe, K. M. Rabe, E. Kaxiras, and J. D. Joannopoulos, Optimized pseudopotentials, Phys. Rev. B **41**, 1227 (1990).

[26] C. T. Van Degrift, Tunnel diode oscillator for 0.001 ppm measurements at low temperatures, Rev. Sci. Instrum. **46**, 599 (1975).

[27] W. A. Coniglio, L. E. Winter, C. Rea, K. Cho, and C. Agosta, Improvements to the tunnel diode oscillator technique for high frequencies and pulsed magnetic fields with digital acquisition, arXiv:1003.5233 (2010).

[28] S. Ghannadzadeh, M. Coak, I. Franke, P. A. Goddard, J. Singleton, and J. L. Manson, Measurement of magnetic susceptibility in pulsed magnetic fields using a proximity detector oscillator, Review of Scientific Instruments **82**, 113902 (2011).

[29] D. E. Graf, R. L. Stillwell, K. M. Purcell, and S. W. Tozer, Nonmetallic gasket and miniature plastic turnbuckle diamond anvil cell for pulsed magnetic field studies at cryogenic temperatures, High Pressure Research **31**, 533 (2011).

[30] http://www.sas.upenn.edu/rappegroup/research/pseudo-potential-gga.html.

[31] B. G. Pfrommer, M. Côté, S. G. Louie, and M. L. Cohen, Relaxation of crystals with the quasi-newton method, J. Comput. Phys. **131**, 233 (1997).

[32] S. Chakravarty, B. I. Halperin, and D. R. Nelson, Two-dimensional quantum Heisenberg antiferromagnet at low temperatures, Phys. Rev. B **39**, 2344 (1989).